A Journal of the Gesellschaft Deutscher Chemiker

Angewandte International Edition

GDCh

Chemie

www.angewandte.org

Accepted Article

Title: Heat-Free Biomimetic Metal Molding on Soft Substrates

Authors: Julia Jinling Chang, Andrew Martin, Chuanshen Du, Alana Pauls, and Martin M. Thuo

To be cited as: *Angew. Chem. Int. Ed.* 10.1002/anie.202008621

Link to VoR: https://doi.org/10.1002/anie.202008621

WILEY-VCH

10.1002/anie.202008621

WILEY-VCH

COMMUNICATION

Heat-Free Biomimetic Metal Molding on Soft Substrates

Julia J. Chang,[a,+] Andrew Martin,[a,+] Chuanshen Du,[a] Alana M. Pauls,[a] and Martin Thuo[a,b,c,*]

[a] Department of Materials Science and Engineering, Iowa State University. Ames, Iowa. 50014. USA
[b] Micro-Electronics Research Centre, Iowa State University. Ames, Iowa. 50014. USA
[c] Department of Electrical and Computer Engineering, Iowa State University. Ames, Iowa. 50014. USA
[*] Corresponding Author
[+] These authors contributed equally to this work.

Supporting information and the ORCID identification

Supporting information for this article is given via a link at the end of the document.

Abstract: Fabrication of bio-templated metallic structures is limited by differences in properties, processing condition, packing, and material state. Herein, we demonstrate that using undercooled metal particles, differences in modulus and processing temperatures can be overcome. Similarly, adoption of autonomous processes like self-filtration, capillary pressure and evaporative concentration leads to enhanced packing, stabilization (jamming) and point sintering with phase change to create solid metal replicas of complex bio-based features. Differentiation of subtle differences between cultivars of the rose flower with reproduction over large areas shows that this BIOmimetic Metal Patterning (BIOMAP) is a versatile method to readily replicate biological features either as positive or negative reliefs irrespective of the substrate. Using rose petal patterns, we illustrate the versatility of bio-templated mapping with undercooled metal particles at ambient conditions, and with unprecedented efficiency for metal structures.

Introduction

Nature is endowed with a plethora of functional surface textures albeit on mechanically delicate or heat sensitive surfaces.[1] These features have evolved, over eons, for protection (e.g. camouflage,[2] or illusion[3]), color (e.g. morpho butterfly[4]) movement (e.g. shark skin[5]), survival in xeric environments[6] (e.g the desert lizard[7] or Namib beetle[8]), among others. Despite their obvious uniqueness and uses, adoption of these biostructures is limited by ability to replicate them, largely due to differences in processing condition needs (e.g. heat for metals).[9] Various efforts to capture these patterns have been limited to replica molding with elastomeric materials[10] or using sophisticated tools for biomimicry on hard materials.[11] The latter is driven by a realization of the utility of biomimetic or analogous patterns on high modulus materials, like metals[12] and ceramics.[13] For example, efforts to create ultra- or superhydrophobic surfaces on hard materials have focused on etching patterns, often using harsh reagents with/without concomitant use of expensive tools and/or skilled labor,[14] with most of these approaches not being amenable to scale up.[15]

Recently, Undercooled metal particles have emerged as a versatile material state.[16] Solvent-suspended polydisperse, soft, non-Hertzian Undercooled Liquid Metal Core-Shell (ULMCS) particles, however, offers the ability to conform, tightly pack, and self-sort through complex multi-scale surface textures such as that of a rose petal (Figure 1a-b). Upon deposition, and solvent evaporation, soft particles tend to form randomly close packed structures (RCP) and jam at a packing factor, ø = 0.64.[17] The packing factor is driven by the relation, $\emptyset = Nv_0/V$, where N is the number of particles, v_0 is unit volume and V is volume. Furthermore, given the existence of multiscale patterns and channels on a rose surface (Figure 1a), these particles would undergo a self-filtration process[18] assisted by capillary self-assembly.[19] Upon drying and reaching a pendular state, they would eventually self-lock and jam within the crevices of the surface textures (Figure 1b). The jamming occurs when inter-particle cavity dimensions, slurry concentration, and particle sizes satisfy the following relation[20]:

$$\frac{R}{r} = \left[\frac{4(n-1)}{3} + 1\right]^{1/2} \qquad [1]$$

Where R is capillary radius, r is particle radius, and n is the number of particles. Equation 1 allows for prediction of size (r) or number (n) of particles needed to jam for a given recess size (R). Relying on the direct dependence on R and n (Equation 1), analogous structures can be readily distinguished based on structure of this jammed state. The jammed state also ensures that deposited ULMCS particles are mechanically stabilized and, therefore, can be sintered into surface-templated conformal networks (Figure 1c-d). Deploying heat-free chemical sintering (the so-called Coalescence of Undercooled Particles through a Chemical Trigger, CUPACT[16d]), joining and solidification of jammed ULMCS particles leads to a solidified structure that can be lifted off without damaging the rose petal or analogous soft substrate. This process is also compatible with synthetic, heat-sensitive and soft, motifs such as PDMS[21] (Figure 1e). When inverse biomimetic structures are templated onto elastomeric materials on which ULCMS particles are packed and chemically sintered, an exact replica of the natural pattern is realized (Figure 1f-h).

Biomimetic solid metallic structures can, therefore, be fabricated without heat by exploiting autonomous processes such as capillary densification (jamming and capillary forces), kinetics frustrated processes (undercooling and CUPACT, Figure S1e-f), and self-assembly/sorting (self-filtration of polydisperse particles, Figure S1c-d) processes. Using undercooled metal particles and associated strain propagation, we demonstrate that a combination of self-filtration and jamming leads to tight packing on a delicate rose petal without inducing damage to the surface. Once densely packed, a chemical sintering process[16d] (Figures S1c-d) locks the particle in place leading to solidification and replication of the structure at a multi-scale level albeit as an inverse of the parent pattern. The envisioned process entails three steps *viz*; i) deposition and densification, ii) activation of solidification, and iii) reveal the replicated structure by lift off. For brevity, we abbreviate this BIOmimetic MetAl Patterning as BIOMAP (Figure 1i).

10.1002/anie.202008621

COMMUNICATION

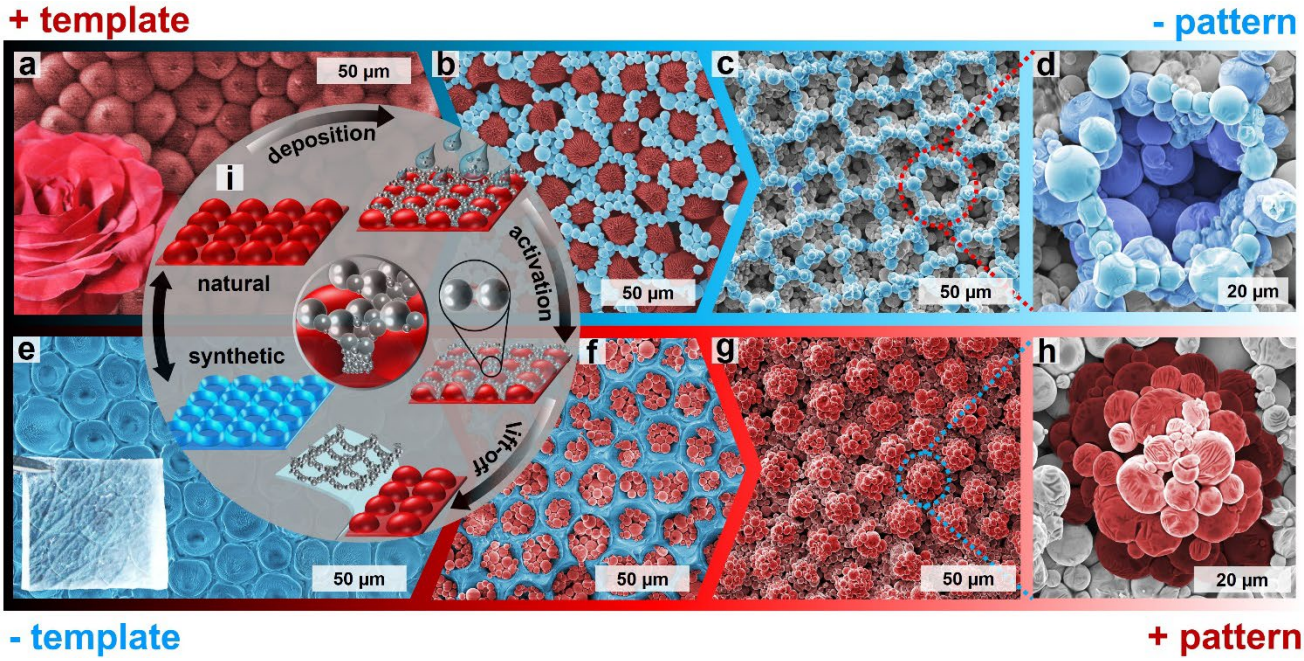

Figure 1. Schematic illustration of heat-free bio-mimetic metal patterning, BIOMAP, with ULMCS. a) Macro- and microstructure of the rose flower template. b) ULMCS jammed into template after deposition and capillary densification. c) Inverse metal rose replica pattern shows the same micro-structure as the rose's Male, (+), template after lift-off. d) Zoom-in of a unit block of inverse metal rose showing effect of self-filtration on particle size distribution. e-h) converting an elastomeric lift-off structure from the rose into a mold, ULMCS deposition, densification leads to conformal packing (f). h) A zoom-in feature of metal rose. i) an overview of the BIOMAP process (false-coloring is used for clarity and to highlight changes in particle sizes in the zoomed in images.)

Results and Discussion

Polydisperse ULMCS Field's metal (51% In, 32.5% Bi and 16.5% Sn w/w) particles were synthesized via the SLICE (Shearing Liquids Into Complex particlEs) method as previously reported.[22] The SLICE process can produce particles < 10 nm, but for enhanced self-filtration and ease of characterization in current study, larger size (µm) and higher polydispersity is desired (see equation 1). Particles used in this study were 2.71 ± 1.58 µm diameter (Figure S1a-b), hence a predicted packing ration of *ca.* ∅= 0.70 based on equation 1 and 2 (see discussion in the SI). These soft deformable ULMCS, as expected, form denser structures than the random close packing observed with hard spheres (∅= 0.64). We infer that the densification is likely due to capillary pressure driven shape change and autonomous size ordering that has been shown to increase densification.[17] These processes, however, can be perturbed by external stresses during particle deposition. To investigate effect of deposition process on packing density, methods with varying degrees of applied shear stress (F_s) were adopted. The particles were deposited on the biological templates, in our case rose petals, and template-stripped using copper tape, creating a biomimetic metallic structure albeit of an inverse relief.

Figure 2a, 2d and 2g schematically shows various deposition methods ranging from low F_s (brushing), high F_s (spin-coating) and no F_s (spraying). The Spraying method is considered to bear minimal F_s as particles are deposited normal to the surface of the petal. Direct brushing method (Figure 2a) induces low F_s on the particle slurry during the deposition resulting in thick (>10 µm), multi-layer (>7 layers) patterns (Figure 2b-c). This method is the most facile, yet the most non-uniform due to user-dependency (i.e. high entropy). Spin coating—dropwise deposition at 1000 rpm (Figure 2d), allows for a more controlled and reproducible deposition process since the shear speed, hence F_s, can fixed. Spin coating, however, shears-off the outermost layer of deposited particles, resulting in slightly thinner films (<10 µm, ~4-5 layers) compared to those obtained through brush-based spreading (Figure 2e-f). Surprisingly, spin coating allows for slightly better self-filtration as shown by autonomous size-sorting on the top layer of the lifted structure (false colored red, Figure 2c vs 2f). The spraying process (Figure 2g), in contrast, gives much thinner films (~3 layers), with significant defects/disconnections (Figure 2h-i). we infer that this is likely due to challenges in pumping the rather dense metallic particles out of the hand spray system, which will bias towards depositing smaller and fewer particles. Sedimentation of larger particles in the solution being sprayed can also contributes to low concentration and size-selectivity hence the generation of thinner films. Although we see smaller particles on the top surface of spray generated structures (Figure 2i) we exercise caution in deducing improved self-filtration in light of the process limitations.

With granular matter, however, self-filtration can lead to better packing into surface features leading to more conformal packing across different size scales. Self-filtration would manifest in size distribution of particles across the topmost layer of captured features. Comparing particle size distribution of the as-prepared particles (Figure S1b) to those that deposit deepest in the rose petal crevices (i.e. presenting as the topmost layer of the metallic features), we observed a significant shift. In the polydisperse parent slurry a large positive skew is observed (Figure S1b), while in the deposited particles, larger particles seem to have been filtered out (Figure 2j-m). Fitting a Gaussian over the distribution of particle sizes of the topmost layer of the lifted off structures shows that brush (~5 µm)>spin-coating (~4 µm)>spray (~3 µm).

10.1002/anie.202008621

Although a general decline is observed, the size differences are within margin of error. Moving to higher statistical moments, however, reveals that the peakedness (kurtosis) drops into negative values indicating smaller tails than a normal distribution (Figure 1m). Kurtosis, therefore, increases with increase in skewness with this rise inversely correlating with magnitude of shear stress F_s and average particle size (Figure 2m). Trend skewness implies that a higher stress may interfere with the self-assembly process by either; i) accelerating carrier fluid removal hence low capillary packing, and ii) compressing the soft ULMCS particles reducing the interparticle pores needed for autonomous size-sorting through self-filtration. Based on the more symmetric distribution in the brush applied patterns (Figure 2j), we infer that moderate amount of stress and slow evaporation of carrier fluid would lead to better packing albeit with potential challenges in scalability. We, therefore, infer that spin-coating, although with a slight relative skewness, is amenable to rapid and scalable fabrication of these features.

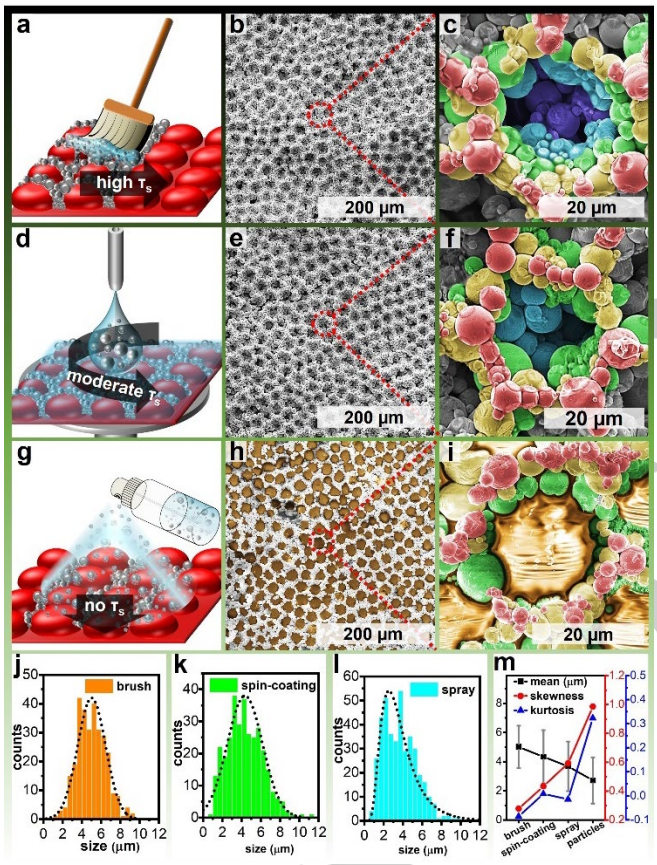

Figure 2. Effect of deposition method on formed features. a) Hand brush (painting) deposition methods, and (b) example of generated replica patterns with c) a zoom-in on one of the patterns. d) Deposition by spin-coating, and e) produced surface features with associated zoom-in f). g) Spray-based deposition and i) associated product, f) where a zoom-in shows shallow features. (for clarity false color highlight different layers: top layer: red, 2nd layer: yellow, 3rd layer: green, 4th layer: blue, 5th layer: purple. Metallic orange represents copper tape.) Size distribution of the top layer particles differentiated by deposition method; brush (j), spin-coating (k) and spray (l) methods. Trends in statistical parameters associated with top-layer and starting particle size distributions (m).

Efficiency of a replication method is best determined by how well the produced features match those of the mold and/or how well the method can distinguish similar structures. To evaluate BIOMAP, we compared size of the radial structures derived from rose petals using different deposition methods (Figure S2). We observe that all features derived from the red rose had an average size in the order brush>spin-coating>spray but all within the margin error of each other and falling around *ca.* 20 µm (Figure S2d). Skewness was also within a margin of error (±0.15) but kurtosis was inversely correlated to F_s (Figure S2).

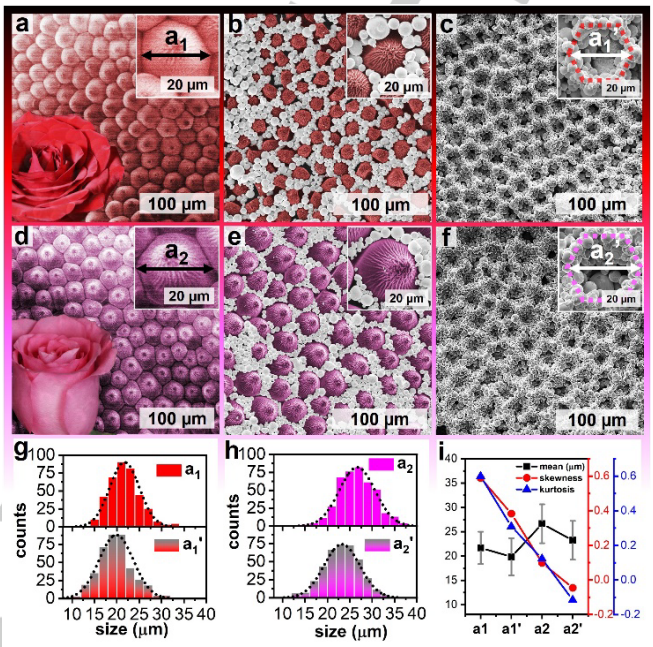

Figure 3. ULMCS biomimetic templating captures fine differences in templates. a) Macro- and microstructure of rose type 1 (red) with feature size labelled as a_1. b) ULMCS deposited onto rose 1 template. c) Activated and lifted-off patterns from rose 1 with pattern feature size labelled as a_1' d-f) Macro/microstructure of a different cultivar, (a_2), ULMCS deposition and pattern feature (a_2') of rose 2 as template. g) a_1 and a_1' distribution. h) a_2 and a_2' distribution. i) Statistical analysis of a_1, a_1', a_2 and a_2'.

To evaluate the resolution of BIOMAP different, but closely related, cultivars of roses were used as the template. Red rose, *Mister Lincoln* hybrid, (rose 1) has a feature diameter, $a_1 = 21.68 \pm 3.32$ µm (Figure 3a). The Pink rose, *Rosa Peace* (rose 2) has a feature diameter, $a_2 = 26.63 \pm 4.00$ µm (Figure 3b). Spin-coating of the same parent slurry onto similarly prepared petals was performed in an effect to capture differences in these templates. Patterns on rose 1 produces patterns with average feature diameter $a_1' = 19.85 \pm 3.82$ µm (Figure 3b-c), a deviation of ~2 µm from the original pattern. We infer that the 10% size difference may emanate from deformation of petal features under capillary pressure and/or weight of deposited particles. For the second rose petal, the average size of templated patterns $a_2' = 23.23 \pm 3.98$ µm (Figure 3e-f), indicating a deviation of ~3 µm from the template. These differences are also captured as shifts in Gaussian means of the resulting histograms (Figure 3g-h). Whereas the shape of the feature size distribution does not change from the petal to the BIOMAP surfaces—indicating good replication, higher moments (skewness and kurtosis) confirm that these subtle changes are systematic errors (Figure 3i). Figure 3i summarizes the average, variance, skewness, and kurtosis, indicating precision and reproducibility of BIOMAP. The ability of BIOMAP to capture subtle differences in two cultivars of the same

10.1002/anie.202008621

plant may open opportunities in structural taxonomy where biological subspecies can be identified through their structure dimensions[23].

Despite the high reproducibility discussed above, all the produced features are inverse reliefs of the natural pattern. Having successfully captured the female (-) version of the rose pattern, we inferred that an analog of the natural rose (male, +) pattern can be obtained by first creating a female mold from an elastomer, PDMS, then using BIOMAP to create a pattern similar to the rose petal. Figure 4 shows how robust BIOMAP is in generating a synthetic rose pattern. First a female (-) template is fabricated through replica molding with PDMS from the rose petal surface (Figure 4a). The PDMS mold is filled with ULMCS particles that are then sintered via CUPACT and patterns lifted-off as described above (Figure 4b-c). A (+) ULMCS pattern is fabricated albeit with larger gaps in between the features compared to the rose flower (Figure 3a), due to retention of sphericity of the particles after CUPACT (Figure S1c-d).

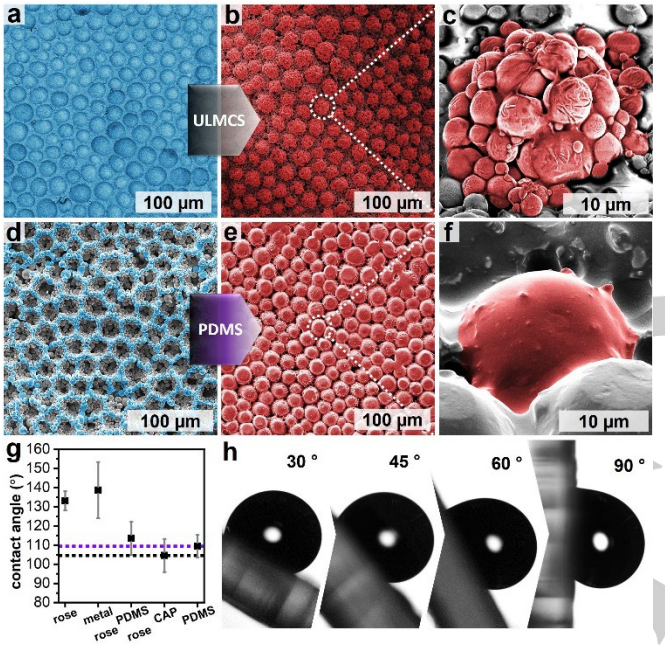

Figure 4. Process of creating a metallic and PDMS rose replica. a) Inverse PDMS rose as the template for creating metallic b) rose replica and c) associated zoom-in. d) inverse metal rose pattern used as a mold for PDMS, f) fabricated PDMS male rose patterns. f) zoom-in feature. g) Static contact angle formed by water droplets on formed surfaces. Difference between analogous structures on rose, metal, and PDMS, referenced to non-patterned PDMS (marked with top dotted line) and chemical activated ULMCS (marked with bottom dotted line). h) droplet shape variation on metal rose surface when the surface is tilted to 30, 45, 60 and 90 degrees.

Despite the limitations in creating a fully continuous smooth surface, we demonstrate the closest analog of a metallic rose surface (Figure 4b) fabricated through physical chemistry and chemical kinetics principles. Besides the new surface texture, we also inferred that the metallic (-) relief replica of the petal surface can be used as a mold to generate an elastomeric analog of the rose petal since capillary forces would inhibit viscous uncross linked elastomer from permeating the pore network. Using our previously fabricated patterns (Figure 4d), we filled the metallic (-) features with PDMS, cross-linked it, and upon lift-off generated a (+) relief pattern analogous to the rose petal—albeit derived from PDMS (Figure 4e-f). Whereas a 10% decrease in feature size was observed when the metal was used to lift-off patterns from the rose petal, there was no significant changes in feature sizes when the metal was used as a mold to create PDMS features (Figure S3a-c) or the rose features were lifted off with PDMS (Figure 4a). These results further confirm our inference that capillary pressure and density difference likely cause the small feature shrinkage. We can, therefore, infer that BIOMAP is a versatile ambient condition method of replicating surface patterns from soft and delicate substrates using metals. Both positive and negative reliefs can be made with a high degree of accuracy and reproducibility, over large areas of surfaces. This enables soft lithography with a higher modulus, stiffer, solvent insensitive, lift off material without damaging the delicate substrate.

Despite the structural differences, however, the wetting properties of the native[24] and replicated rose patterns are comparable. Figure 4g shows similarity in hydrophobicity measured through contact angle of water droplets on the biomimetic surface. The as purchased rose petal was ultra-hydrophobic with an average contact angle of 133.1 ± 5.0 ° whereas the biomimetic replica, (+) ULMCS pattern (Figure 4b), gave an average contact angle of 138.7 ± 14.7°. The PDMS rose replica showed a lower contact angle of 115° (Figure 4g). Non-textured CUPACT sintered particles (CAP, Figure 4g) and cured PDMS were used as references (Figure 4g, dotted lines). Droplets on untextured sintered particle surfaces slowly diffused into the porous surface shows transient hydrophobicity. We infer the slight hydrophobicity observed on the sintered particle bed to be due to the presence of an essential methyl terminated surface ligand used to stabilize ULCMS. To further compare the wetting between the biomimetic and nature patterns, we tilted the droplets sitting on BIOMAP rose pattern (Figure 4b) to illustrate the petal effect (Figure S3d-g). We observe that, as expected, the droplet adheres to the surfaces albeit with a large contact angle hysteresis with increase in tilt angle (Figure 4h and supporting video).

Conclusion

In conclusion, we demonstrate a method to fabricate biomimetic metallic patterns from delicate soft substrates, herein a rose petal. Exploiting versatility of the SLICE method to prepare ULMCS particles, resolution in replication can be improved by incorporating smaller particle sizes. The fabricated features closely mimic the bio-analog both in structure and wetting properties albeit with subtle diversions, artefacts of the BIOMAP processing method and asymmetry in material properties. Replication of the patterns with BIOMAP shows high accuracy and reproducibility, illustrating that ambient autonomous process can be used to overcome challenges in processing conditions. We hypothesize that BIOMAP, being compatible with a wide range of working conditions may find use in structural anatomy i.e. identification of variants based on differences in expressed features as demonstrated here with rose petals or in structural materials where controlled wetting has implication in diverse fields as corrosion and heat transfer. BIOMAP advances soft lithographic methods by employing physical-chemical (CUPACT, jamming, undercooling, capillary densification) processes.

Acknowledgements

This work was supported by Iowa state university through intellectual property royalty funds to MT. The authors thank Dr. Warren Straszheim (SEM) for technical assistance.

Conflict of interest

The authors declare no conflict of interest.

Keywords: biomimetic • soft lithography • self-filtration • heat-free • ultra-hydrophobic

[1] a) B. Bhushan, Phil. Trans. R. Soc. A, **2009**; b) J. P. Vigneron, P. Simonis, *Physica B* **2012**, *407*, 4032-4036.
[2] J. Teyssier, S. V. Saenko, D. Van Der Marel, M. C. Milinkovitch, *Nat. Commun.* **2015**, *6*, 6368.
[3] B. Larison, R. J. Harrigan, H. A. Thomassen, D. I. Rubenstein, A. M. Chan-Golston, E. Li, T. B. Smith, *R. Soc. Open Sci.* **2015**, *2*, 140452.
[4] a) B. Song, V. E. Johansen, O. Sigmund, J. H. Shin, *Sci. Rep.* **2017**, *7*, 46023; b) G. D. Bixler, B. Bhushan, *Soft matter* **2012**, *8*, 11271-11284.
[5] S. Wainwright, F. Vosburgh, J. Hebrank, *Science* **1978**, *202*, 747-749.
[6] N. G. Jablonski, G. Chaplin, *PNAS* **2010**, *107*, 8962-8968.
[7] K. Autumn, Y. A. Liang, S. T. Hsieh, W. Zesch, W. P. Chan, T. W. Kenny, R. Fearing, R. J. Full, *Nature* **2000**, *405*, 681-685.
[8] W. J. Hamilton, M. K. Seely, *Nature* **1976**, *262*, 284-285.
[9] a) W. Jiang, M. Mao, W. Qiu, Y. Zhu, B. Liang, *Ind. Eng. Chem. Res.* **2017**, *56*, 907-919; b) A. H. Cannon, W. P. King, *J Micromech Microeng* **2009**, *19*, 095016.
[10] a) G. Wen, Z. Guo, W. Liu, *Nanoscale* **2017**, *9*, 3338-3366; b) M. Karaman, N. Çabuk, D. Özyurt, Ö. Köysüren, *Appl. Surf. Sci.* **2012**, *259*, 542-546.
[11] a) O. I. Vinogradova, A. L. Dubov, *Mendeleev Commun.* **2012**, *22*, 229-236; b) S. Oyola-Reynoso, I. Tevis, J. Chen, B. Chang, S. Çinar, J.-F. Bloch, M. M. Thuo, *J. Mater. Chem. A* **2016**, *4*, 14729-14738.
[12] S.-w. Ryu, S. Choo, H.-J. Choi, C.-H. Kim, H. Lee, *Appl. Surf. Sci.* **2014**, *322*, 57-63.
[13] a) T. Liu, C.-J. Kim, *Science* **2014**, *346*, 1096-1100; b) L. Cao, H.-H. Hu, D. Gao, *Langmuir* **2007**, *23*, 4310-4314; c) M. Karlsson, P. Forsberg, F. Nikolajeff, *Langmuir* **2010**, *26*, 889-893.
[14] a) C. Frankiewicz, D. Attinger, *Nanoscale* **2016**, *8*, 3982-3990; b) J. K. Park, Z. Yang, S. Kim, *ACS Appl. Mater. Interfaces* **2017**, *9*, 33333-33340; c) H. Toyota, K. Takahara, M. Okano, T. Yotsuya, H. Kikuta, *Jpn. J. Appl. Phys.* **2001**, *40*, L747.
[15] K. Uchida, R. Nishimura, E. Hatano, H. Mayama, S. Yokojima, *Chem. Eur. J.* **2018**, *24*, 8491-8506.
[16] a) S. Çınar, I. D. Tevis, J. Chen, M. Thuo, *Sci. Rep.* **2016**, *6*, 1-12; b) B. S. Chang, R. Tutika, J. Cutinho, S. Oyola-Reynoso, J. Chen, M. D. Bartlett, M. M. Thuo, *Mater. Horizons.* **2018**, *5*, 416-422; c) B. S. Chang, M. Fratzl, A. Boyer, A. Martin, H. C. Ahrenholtz, I. De Moraes, J.-F. Bloch, N. M. Dempsey, M. M. Thuo, *Ind. Eng. Chem. Res.* **2019**, *58*, 4137-4142; d) A. Martin, B. S. Chang, Z. Martin, D. Paramanik, C. Frankiewicz, S. Kundu, I. D. Tevis, M. Thuo, *Adv. Funct. Mater.* **2019**, *29*, 1903687.
[17] A. Donev, I. Cisse, D. Sachs, E. A. Variano, F. H. Stillinger, R. Connelly, S. Torquato, P. M. Chaikin, *Science* **2004**, *303*, 990-993.
[18] S. D. Kulkarni, B. Metzger, J. F. Morris, *Phys. Rev. E* **2010**, *82*, 010402.
[19] a) E. P. Lewandowski, M. Cavallaro Jr, L. Botto, J. C. Bernate, V. Garbin, K. J. Stebe, *Langmuir* **2010**, *26*, 15142-15154; b) J. Xu, J. Xia, S. W. Hong, Z. Lin, F. Qiu, Y. Yang, *Phys. Rev. Lett.* **2006**, *96*, 066104; c) N. Bowden, I. S. Choi, B. A. Grzybowski, G. M. Whitesides, *J. Am. Chem. Soc.* **1999**, *121*, 5373-5391; d) Y. Lin, E. Balizan, L. A. Lee, Z. Niu, Q. Wang, *Angew. Chem. Int. Ed.* **2010**, *49*, 868-872.
[20] a) S. Yang, J. R. Evans, *Powder Technol.* **2004**, *139*, 55-60; b) R. P. Behringer, B. Chakraborty, *Rep. Prog. Phys.* **2018**, *82*, 012601.
[21] S. Dai, Y. Zhu, Y. Gu, Z. Du, *Appl. Phys. A* **2019**, *125*, 138.
[22] I. D. Tevis, L. B. Newcomb, M. Thuo, *Langmuir* **2014**, *30*, 14308-14313.
[23] a) D. Potter, T. Eriksson, R. C. Evans, S. Oh, J. Smedmark, D. R. Morgan, M. Kerr, K. R. Robertson, M. Arsenault, T. A. Dickinson, *Plant Syst. Evol.* **2007**, *266*, 5-43; b) K. Koch, B. Bhushan, W. Barthlott, *Soft Matter* **2008**, *4*, 1943-1963.
[24] M. Nosonovsky, B. Bhushan, in *Green Tribology*, Springer, **2012**, pp. 25-40.

10.1002/anie.202008621

WILEY-VCH

COMMUNICATION

Entry for the Table of Contents

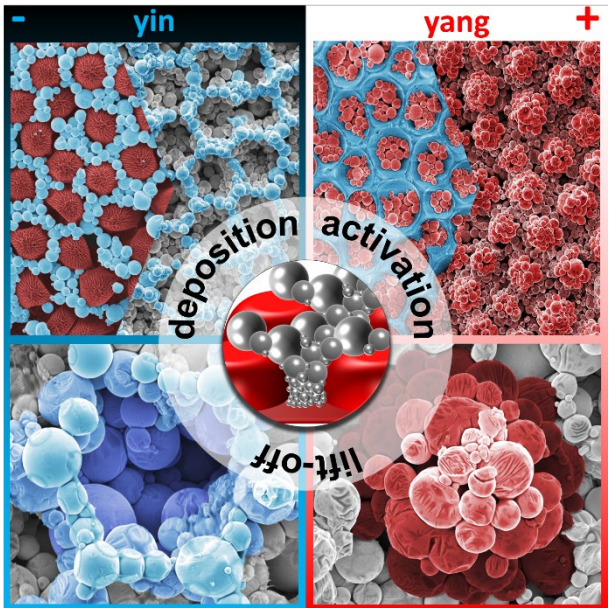

The Yin-Yang BIOMAPing: By exploiting packing, jamming, self-filtration and kinetics, we developed a heat-free biomimetic metal patterning (abbreviated BioMAP) using delicate rose petals. Rose-like structures, both inverse (yin/-) as well as direct (yang/+), were successfully replicated using undercooled liquid metal core shell particles. This method created textured metal patterns with great accuracy, and reproducibility such that patterns from closely related cultivars can be differentiated. Like the parent, both structure and wetting properties are conserved.

Institute and/or researcher Twitter usernames: @smmtgroup